

# An open Platform for High-resolution Light-based Control of Microscopic Collectives

Ana Rubio Denniss<sup>1</sup>, Thomas E. Goroehowski<sup>1</sup>, and Sabine Hauert<sup>1</sup>

<sup>1</sup>Affiliation not available

January 11, 2022

## Abstract

Engineering microscopic collectives of cells or microrobots is challenging due to the often-limited capabilities of the individual agents, our inability to reliably program their motion and local interactions, and difficulties visualising their behaviours. Here, we present a low-cost, modular and open-source Dynamic Optical MicroEnvironment (DOME) and demonstrate its ability to augment microagent capabilities and control collective behaviours using light. The DOME offers an accessible means to study complex multicellular phenomena and implement de-novo microswarms with desired functionalities.

Corresponding author(s) Email:

[thomas.goroehowski@bristol.ac.uk](mailto:thomas.goroehowski@bristol.ac.uk) [sabine.hauert@bristol.ac.uk](mailto:sabine.hauert@bristol.ac.uk)

## ToC Figure

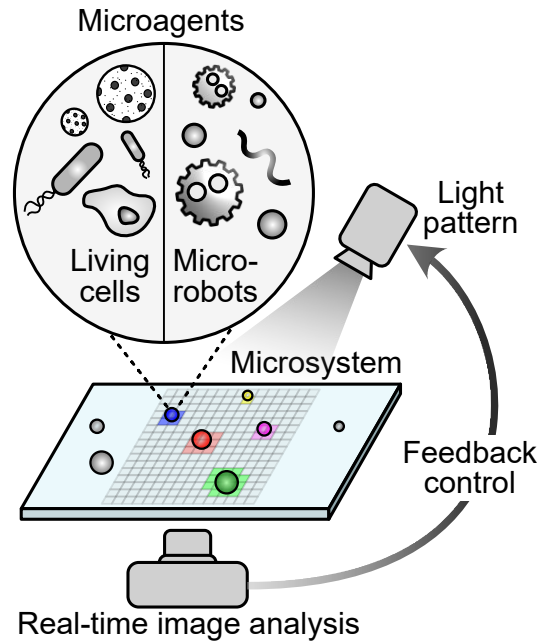


Figure 1: **ToC Figure.** Through the integration of real time image analysis and digital light processing, an optical microenvironment is shaped around the evolving dynamics of a microsystem. Structured light is output by a projection unit onto the microsystem, which could consist of agents such as microparticles, algae or mammalian cells. The response of these agents is captured by a microscopy and camera set up.

## Introduction

Self-organisation is used by many biological systems to drive the emergence of robust collective phenomena across large populations of cells, and is known to underpin processes such as tissue morphogenesis, collective motion and disease progression (Gorochowski et al., 2020). Engineering microagents – be they living cells or human-made microrobots – with similarly complex collective behaviours would have applications ranging from the design of new functional materials (Slavkov et al., 2018) to novel biomedical therapies (Alapan et al., 2019; Hauert and Bhatia, 2014). The key component driving self-organisation is the ability for agents to react to their local environment and follow simple behavioural rules (Brambilla et al., 2013). However, at present we struggle to rapidly tweak the rules that microagents follow. As a stepping stone, in this work we propose to externally control each microagent and their reaction to the local environment, allowing for the rapid prototyping of behavioural rules that give rise to self-organisation. Light is perfectly suited for this task and at small scales can be used to make and break bonds (Chen et al., 2018), power micromotors (Palagi et al., 2019), alter shapes (Stoychev et al., 2019), drive the release of a cargo (Erkoc et al., 2018), modify microenvironments (Ruskowitz and DeForest, 2018), and interact with light sensing organisms (Jékely et al., 2008; Purcell and Crosson, 2008), making it a powerful tool for microagent control. Moreover, unlike other methods based on the use of chemicals or magnetic fields, light is better suited to the simultaneous control of many agents due to its high spatio-temporal resolution.

Light-controlled microswarms have been shown to perform collective phototaxis (Dai et al., 2016), self-assemble into active materials (Schmidt et al., 2019), and treat tumours (Tao et al., 2020), yet many of these systems rely on manual control of a single or few light stimuli, offering limited local control at the scale of large collectives. In a number of instances, closed-loop high-resolution spatio-temporal control has been demonstrated, achieving complex behaviours such as flocking (Lavergne et al., 2019), formation of sophisticated shapes (Frangipane et al., 2018) and collective cargo transport (Steager et al., 2015). However,

typically a bespoke optical set up is needed to realise this control, making the approach inaccessible to most labs. Of the set ups that have been previously developed, very few are reproducible due to insufficient documentation, and many rely on components such as optical breadboards (Lam et al., 2017) or fluorescence microscopes (Stirman et al., 2012) to provide structural and mechanical functions, which can be costly and may require some degree of specialised expertise to install and operate.

To address these limitations, here we present the Dynamic Optical MicroEnvironment (DOME). The DOME is a fully integrated device that is able to project dynamic light patterns in response to the behaviour of light-reactive microagents and guide their collective behaviour (Figure 1). This is made possible by the DOME’s ability to continuously image a microsystem and use this information as input into feedback control schemes that can then modify the light pattern projected in real-time to interact and guide the behaviours of the individual agents. Furthermore, the DOME has been specifically designed to be low-cost, modular, and open source to allow for the easy adaptation to new applications. This builds on other existing open platforms focused on microscopy, by adding fine-grained light-based control (Diederich et al., 2020).

## Materials and methods

The DOME (Figure 2) consists of three major subsystems: dynamic light projection, real-time imaging, and computation of feedback control signals. The imaging module, which consists of an inverted microscopy set up and camera, observes changes in the micro-system such as agent density or position, and communicates these changes to the projection module via feedback control. This causes the projected light to be restructured in line with the new state of the system, creating what we term a ‘light-based augmented reality layer’ (Denniss et al., 2019) on the sample stage that can be used to influence the behaviour of light-responsive microagents that are present.

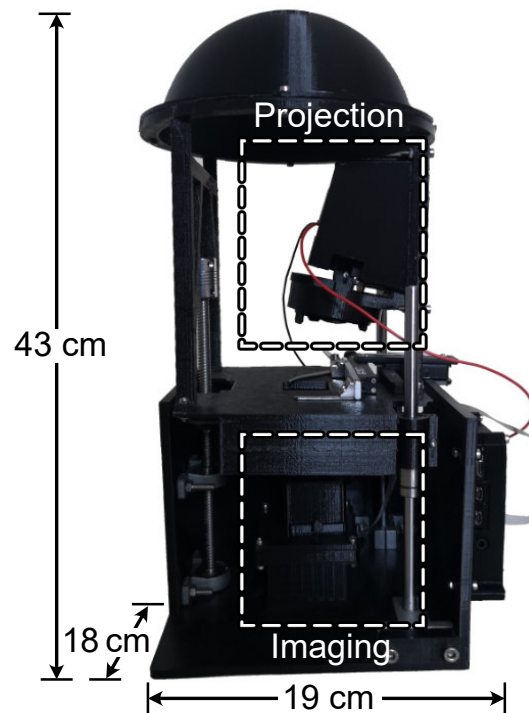


Figure 2: Fully assembled DOME with dimensions.

Achieving closed loop control within the DOME requires the integration of optical and computational pathways, as represented in Figure 3. Light patterns from the projector pass through a condenser lens and onto the sample stage. The sample is imaged through a column containing a magnifying tube lens, filters for fluorescent imaging (if required), and finally a microscope objective.

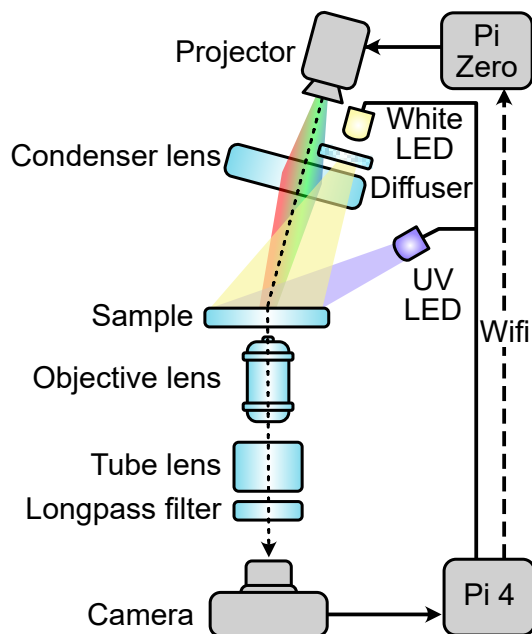


Figure 3: Schematic of key components and their connection within the DOME. Optical components are coloured light-blue, and arrows depict the flow of information. Dotted lines denote the optical path and dashed lines are wireless communication links.

Images are captured by a Raspberry Pi 4 with camera module, which performs real-time image analysis. The Raspberry Pi 4 is also used to control LEDs for bright field and fluorescence imaging, and is designed to run analysis code for generating control signals (i.e. the light pattern to be projected). Furthermore, this module is configured as a node in a local ad-hoc network to which a Raspberry Pi Zero is also connected. The Raspberry Pi Zero acts as a controller for the projector and is constantly fed information from the imaging process running on the Raspberry Pi 4 through this wireless communication channel. This enables closed-loop control as properties of the system being imaged (e.g. agent location or density) can influence the light pattern being projected.

## Fabrication of the DOME

The DOME is an assembly of parts 3D printed in PLA plastic (Figure 4), together with low cost optical, mechanical and electronic components (Figure 5). The original device was printed using an Ultimaker 2+ printer, and has been replicated using an Anycubic i3 Mega, a lower budget machine. Parts were designed using Autodesk software and can be printed without requiring dissolvable supports.

Z-plane focusing is achieved using a linear rod set, where manually rotating the lead screw raises or lowers the sample stage with respect to the imaging lens and camera. An x-y translational stage is attached to the sample stage to allow smooth sample adjustment in this plane. This affects only the positioning of the

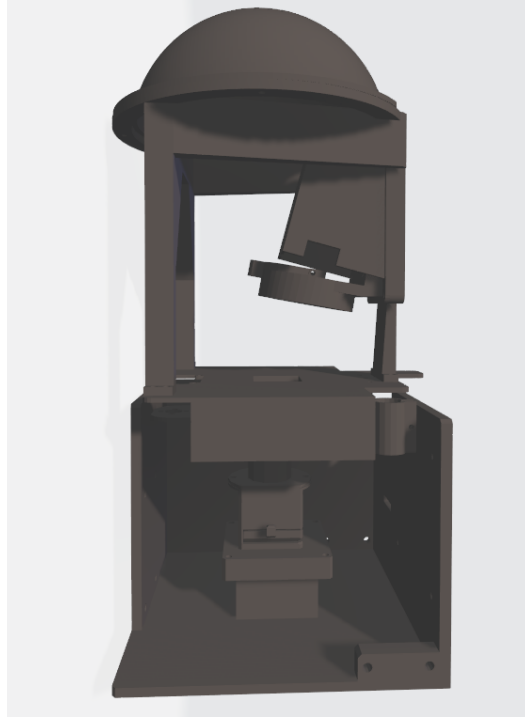


Figure 4: 3D assembly of the DOME parts.

sample and has no bearing on the relative positions of the optical components. The imaging column faces upwards towards the sample stage from the base of the DOME and contains an optical filter holder on a pivot hinge and printed internal threads to attach magnification lenses. The imaging column has two different attachments that can be used, one for a lower magnification option in which only a tube lens is required, and an extended version for higher magnification, where a microscope objective can be attached.

## Optical set up

To control microscale collectives, the DOME must be capable of both visualising these agents and targeting them with localised light. This necessitates combining together projection and microscopy optical pathways. The precise configuration of critical optical components is given in Figure 6.

The digital light projector (DLP) module is fixed on the sample stage, and thus is unaffected by any adjustment in z-plane focus. It is instead focused independently using a screw lever attached to the projector. Light from the projector is focused by a condenser lens (50 mm diameter PCX condenser lens, Edmund Optics), resulting in a total projection size of  $14.5 \times 26$  mm. A white LED (RS Components) can also be attached behind the condenser lens to act as a bright-field light for standard microscopy. To provide an illumination across the sample, a ground glass diffuser (Thor Labs) is placed between the LED and condenser lens. It is additionally possible to attach a UV LED for fluorescence imaging. Note that although the DOME is capable of bright-field and fluorescence illumination, these features were not used in the experiment presented here. A camera (Camera Module V2, Raspberry Pi) sits on the base of the imaging column and is pointed upwards towards the sample stage. Optics such as wavelength or neutral density filters can be added into the optics holder within the imaging column on an application specific basis. For the lower magnification configuration, the imaging column ends with a 9X tube lens (Eyepiece Cell Assembly, Edmund Optics) screwed into a threaded cylindrical casing. For higher magnification applications the cylindrical section is extended, ending in an RMS thread to fit a standard microscope objective (finite conjugated 10X Semi-Plan

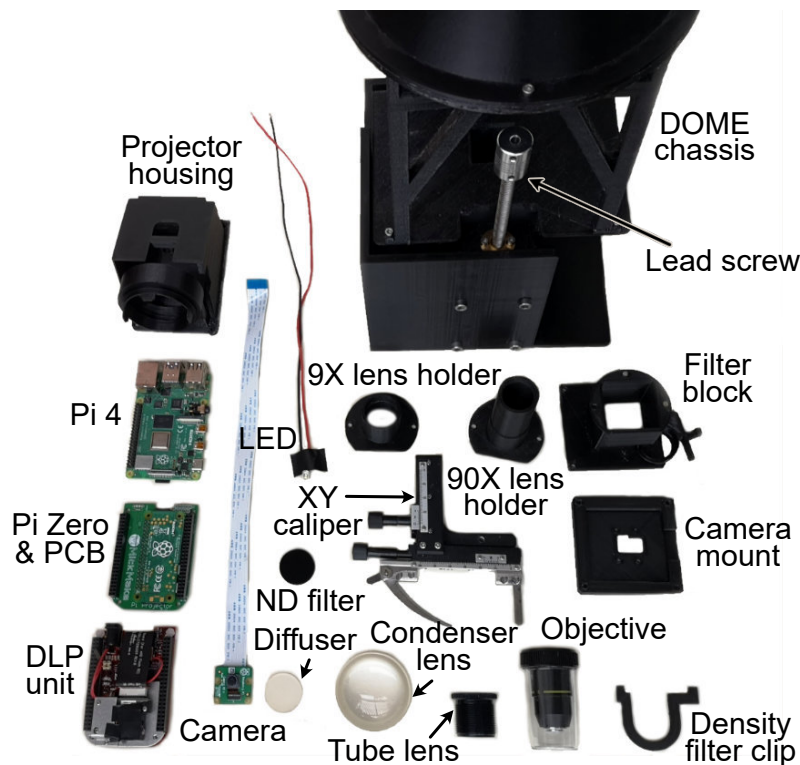


Figure 5: Dismantled DOME with all key components labelled.

Standard Objective, Edmund Optics). While the length of this lens piece is specific to the lenses used here, due to the modular nature of the DOME it would be trivial to adjust this dimension to suit alternative optics. Positioning both the camera and projector perpendicular to the sample stage results in significant lens flare through which imaging is difficult. To circumnavigate this the projector is angled at  $10^\circ$ , positioning the bright spot created by the light source of the projector out of the camera field of view (FOV).

## Characterisation of imaging and projection modules

The modular design of the DOME allows for interchangeable levels of magnification using a tube lens and an RMS threaded tube to mount different microscope objectives. A low magnification of 9X is suitable for larger microsystems of the order of hundreds of microns in size such as multi-cellular algae, while a higher magnification of 90X is appropriate for smaller agents such as mammalian cells or bacteria.

To assess the imaging and projection capabilities, we began by comparing the 9X and 90X magnification settings and used *Volvox* as an example subject. *Volvox* are an algae 350–500  $\mu\text{m}$  in diameter where a single spherical colony houses up to 50,000 cells. At 9X magnification, many colonies can be seen in low detail whereas at 90X magnification only a few are visible but smaller features such as daughter colonies within the body of each *Volvox* are clearly seen (Figure 7). A scale for both magnifications was calculated by imaging a measuring ruler.

Next, we considered light projection. Light projection is performed by a digital light projector that creates a controllable grid of  $854 \times 480$  pixels (0.4 megapixels). When light from the projector is focused through the condenser lens, the total projection area on the sample stage is  $14.5 \text{ mm} \times 26 \text{ mm}$ , making each projected pixel theoretically  $30 \times 30 \mu\text{m}$  in size. Due to differing FOVs for each magnification, this fixed projection area leads to a trade-off with the number of projected pixels that are visible to the camera ( $300 \times 300$  pixels

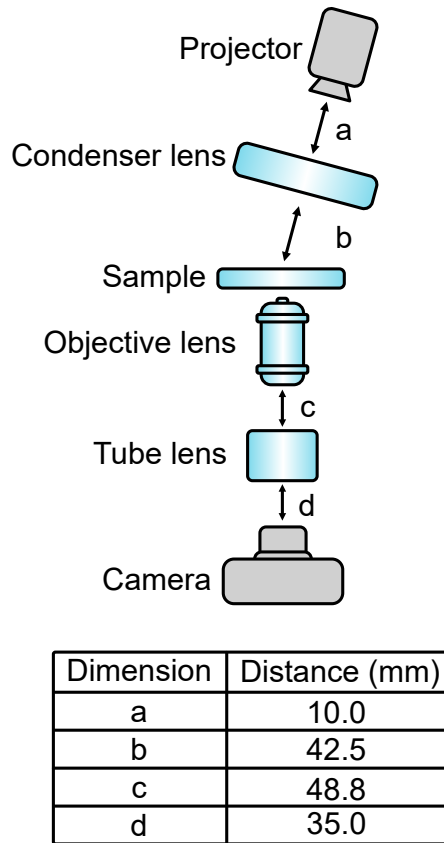


Figure 6: Precise optical configuration of the DOME detailing the spacing between optical components that combine projection and imaging pathways.

for 9X , and  $88 \times 66$  pixels for 90X magnification).

To test the precision of projected light patterns, a series of line triplets of differing size and spacing were projected onto a neutral density filter (Figure 8). The resulting camera images were then analysed by averaging the intensity for each pixel row. High precision projected patterns would result in clear differences in light intensity for even closely spaced lines.

## Light spectra measurements

Another key feature of the DOME is the ability for each projected pixel to have a different colour. This offers the means to provide multiple light-signals to different agents and supports multiplexed communications for more complex behavioural control. This capability is possible due to the projector containing three separate LEDs for red, green and blue light. As living microagents are often sensitive to specific wavelengths of light, we characterised the light spectra of each LED separately. The light spectra produced by the projection module was performed using a calibrated spectrophotometer (Ocean Optics). To collect the readings the optical fibre used for measurement was attached to the DOME at the sample plane facing upwards. The projector was set to a full screen display where all pixels had value (0, 0, 255), (0, 255, 0) or (255, 0, 0) respectively for red, blue and green.

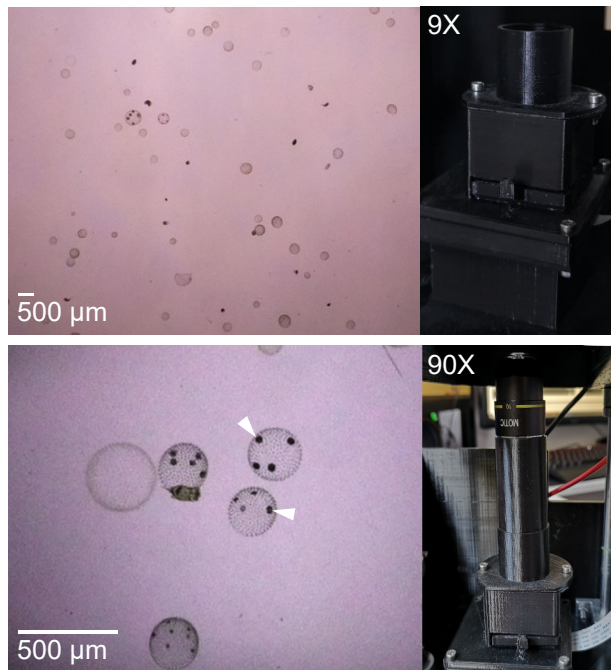


Figure 7: This is a *Volvox* colonies imaged through a 9X magnification lens (top) and 90X magnification lens (bottom). White arrows show daughter *Volvox* colonies. Images on the left show the optical setup for each configuration. caption

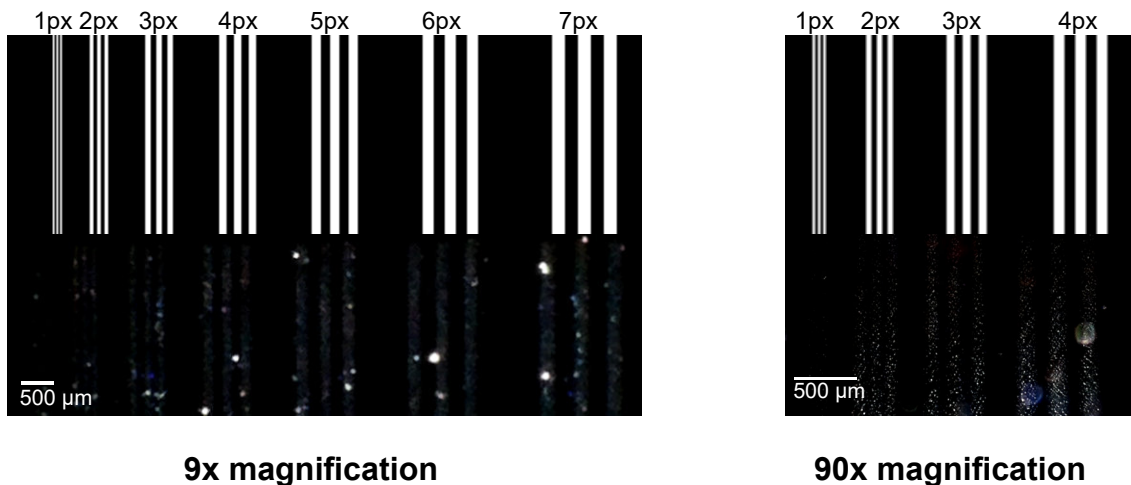


Figure 8: Characterisation of projection and imaging modules. Projection image of line triplets of increasing width up to 7 pixels for 9X magnification (left) and 4 pixels for 90X magnification (right).

### Latency of closed-loop control schemes

For effective closed-loop control, the latency between the imaging of the sample and resulting light projection should be minimised. For the DOME, latency can be described as the time period between subsequent camera frames being obtained, since a new frame is captured only after the imaging module has sent data to the projection module and received confirmation of its receipt. The system latency will vary between applications

and depends on camera settings, and the amount of image processing required per frame. To characterise the baseline latency of the DOME, an experiment was run with no image processing where the projector was switched between an on (white) and off (black) state after every camera frame received. We found that the primary source of latency was the time needed by the camera to capture an image, which is also dependent on the capture resolution. The algorithm was therefore run over a range of resolution settings. Each time measurement was taken as a mean average over 100 frames, running at a shutter speed of 100 milliseconds. Measurements were taken at 63 different resolution settings, starting at  $640 \times 480$  pixels and increasing in increments of  $32 \times 32$  pixels until maximum camera resolution was reached at  $2646 \times 2464$  pixels.

## Closed-loop computational set up

The projection module is comprised of the DLP LightCrafter Display 2000 Evaluation Module (Texas Instruments) interfaced through a custom PCB (Pi Zero W adapter board, Tindie) with a Raspberry Pi Zero W. The imaging module comprises a Raspberry Pi 4, Raspberry Pi camera and illumination LEDs. This computer acts as the primary computing module and user interface, and can be connected to a monitor, mouse and keyboard, or accessed remotely. Crucial to the closed-loop control scheme of the DOME is two-way communication between the imaging and projection module. Due to the interface between the Raspberry Pi Zero and DLP unit there are no ports available to facilitate a physical connection. As an alternative, the two Raspberry Pi modules are configured as nodes in an *ad-hoc* wireless network. The network was established by editing the network interface files on both Raspberry Pi computers to include details of the required *ad-hoc* connection and IP addresses for both nodes. This ad hoc configuration allows the two-way transfer of information for closed-loop control, with the imaging module operated as a server, and the projection module connecting as a client. The connection also enables the user to control the projection module from the imaging module via a VNC connection. With the projection module Pi running VNC server and the imaging module Pi running VNC Viewer, both desktops can be accessed and controlled using a single desktop, mouse and keyboard set up if needed.

## Calibration algorithm for the camera and projector

Due to the nature of using a square camera sensor to image through a circular imaging column and lenses, raw camera images contain sizable “dead space” (an area containing no information). A raw camera frame will appear as a black rectangle with a circular area in the centre in which the sample is visible. To increase image processing efficiency and reduce file sizes, the first step in the calibration process is to crop the total FOV down to a rectangular area that fits inside the circular area of visibility. For this, contour detection is run to find the illuminated area. From these coordinates, the largest square is found by contour detection and this information is written to a file in the format (centre-x, centre-y, width, height). This file can then be imported by all other programs to maintain consistency. Critical to the operation of the DOME is the ability to translate coordinates within the camera frame of reference into the corresponding projector coordinates. For this, the camera space is mapped to the projector space through a calibration process. The first step is to locate approximately where in the projector space the camera is focused using an iterative quadrant search. Once the appropriate sub-space has been found, a 4-point square is projected into this area and located in the camera frame using contour detection. With these sets of coordinates for the projector and camera spaces, the parameters for a matrix transformation operation can be extracted. The baseline code for calibration is provided as part of the open-source DOME software.

## Agent imaging and tracking

The Raspberry Pi Camera was used for all imaging, operating at a resolution of  $1920 \times 1088$  pixels. In all cases, exposure mode was set to ‘spotlight’ and camera ISO was set to 100, with a shutter speed of 200 ms. The camera was operated using the capture continuous method in which images are captured in an infinite loop, iterating over frames. A neutral density filter (NE510B-A, Thor Labs) was also used to minimise

optical interference artifacts. All image processing and projection algorithms were developed using Python and executed through the Raspberry Pi OS. *Volvox* agents were detected in the camera FOV by finding image contours using OpenCV and filtering for size and compactness. ID based tracking was implemented by matching the locations of contours in a given frame to those in the previous frame. Agents were matched to their most likely ID by checking their current location against agents in the previous frame. The closest match was assumed to be the same agent, provided that the distance between the two locations was smaller than 35 pixels (420  $\mu\text{m}$ ). This method was largely effective in locating and matching agents. However, we found it did not always reliably distinguish agents where two or more collided. This issue was, for the most part, minimised by the relatively low density of *Volvox* in the FOV at any one time. Where this issue did occur, the tracking system is designed to assign new IDs to the agents once separated to avoid data becoming biased by these events.

## Agent illumination

*Volvox* samples (Blades Biological, UK) were maintained at room temperature. For imaging, 75  $\mu\text{L}$  of the *Volvox* suspension was added to the sample arena, comprised of 3D printed walls attached to a microscope slide (Figure 9). This sample arena was constructed to allow the free movement of *Volvox* colonies. A square chip of outer dimensions  $25 \times 25 \text{ mm}$  with a  $7.75 \times 7.75 \text{ mm}$  square cut from the middle was 3D printed in PLA and attached to a standard glass microscope slide using superglue adhesive. This square well has depth of 1.5 mm, allowing *Volvox* colonies of 350–500  $\mu\text{m}$  in diameter to move freely in the  $x$ - $y$  plane, with some limited movement in the  $z$  plane.

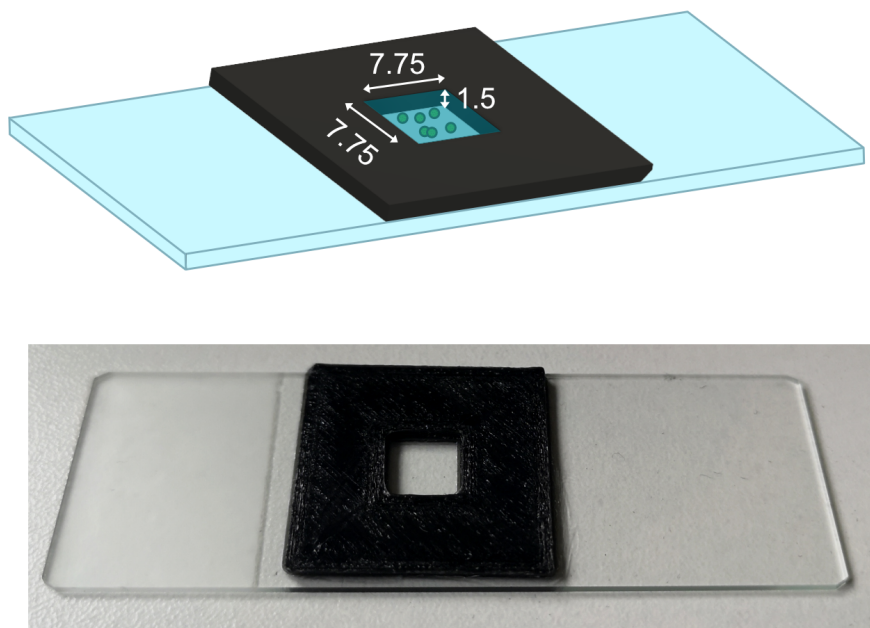


Figure 9: Sample area to facilitate the free movement of *Volvox*. Arena is comprised of 3D printed walls glued to a microscope slide.

During experiments with *Volvox*, samples were uniformly illuminated with a low-level red light. Due to the off-axis projection, this produced images of *Volvox* agents that appear bright red against a dark background, as opposed to bright-field imaging in which agents are dark against a brightly lit background. Keeping background light levels low in this way, and using red light minimises the effect of background light on *Volvox* agents, which respond much more strongly around the 500 nm wavelength range. A typical projection image

was a uniformly dark red background, RGB pixel values (50, 0, 0), with coloured patterns at a brighter intensity. Light patterns were generated based on agent location coordinates, sent as a JSON formatted data to the projection module after translated from camera to projector space.

## Results and discussion

### Characterisation

As detailed in **Materials and Methods**, a detailed characterisation of the DOME was performed to assess its capabilities. Calibrated measurements showed that 1 pixel in the camera field of view (FOV) equated in the real-world to  $12 \times 12 \mu\text{m}$  at 9X magnification, and  $3.75 \times 3.75 \mu\text{m}$  at 90X magnification .

To calculate the projection resolution, line triplets of varying thicknesses were projected and imaged (Figure 8). The resulting intensity analysis (Figure 10) shows that for 9X magnification, lines of 1 pixel width were observable although somewhat difficult to distinguish due to low intensity levels, with more distinct lines can be seen at separations of 2 pixels or more. The same can be seen for the 90X magnification results. Measuring across the peaks allows direct measurement of the observed projector pixel size. At both magnifications this agrees with the theoretical projector pixel size of  $30 \times 30 \mu\text{m}$ .

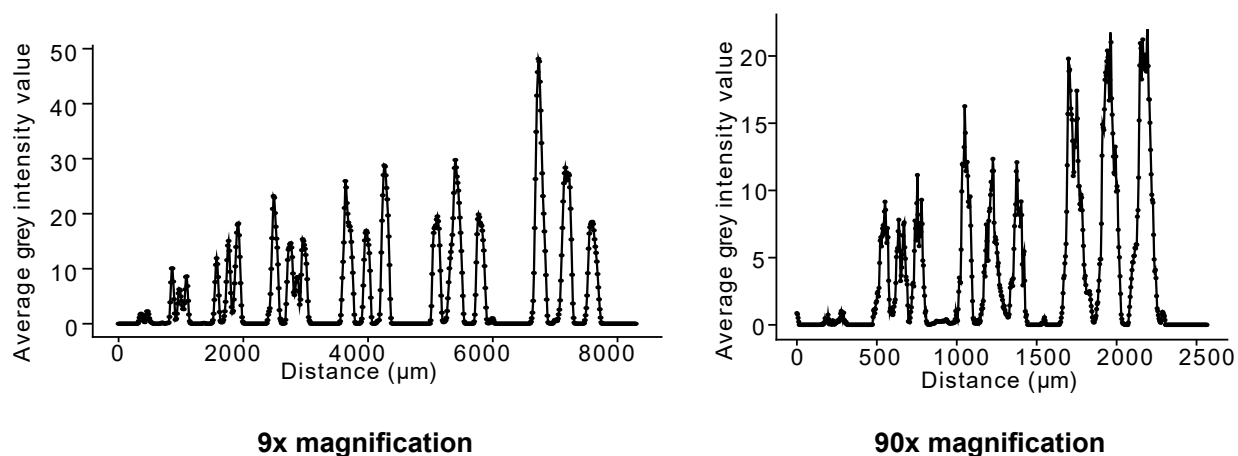


Figure 10: Intensity plot across test image for 9X (left) and 90X (right) magnification, measured as the average grey-scale value for each pixel column in the image.

We also assessed the light spectrum from the digital light projector and found that at full intensity it contained peaks at 460 nm, 510 nm and 640 nm corresponding to the red, green and blue (RGB) LEDs within the projector (Figure 11). Little overlap was observed between each of the LEDs' emission spectra (<2%) making them suitable for multiplexed communication to individual agents (i.e. using each colour as a separate channel).

For feedback control, the time taken to image the microsystem, calculate a light pattern, project it and sense this change is crucial. We found that the camera resolution was the key determinant of latency, which increased with imaging resolution . To measure the baseline latency of the DOME, the device was run with no image processing (as this would vary depending upon the experiment performed) to assess the inherent time taken for imaging and projection. The results showed that even for the highest resolutions, we are able to close the loop in under one second (Figure 12).

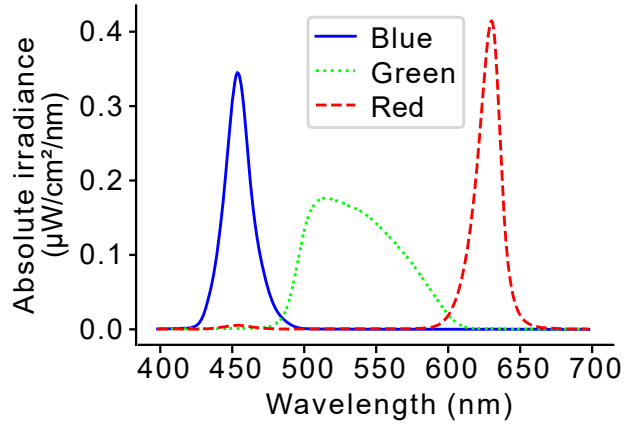


Figure 11: Spectra of light emission from the projection module showing clear separation of the red, green and blue LEDs.

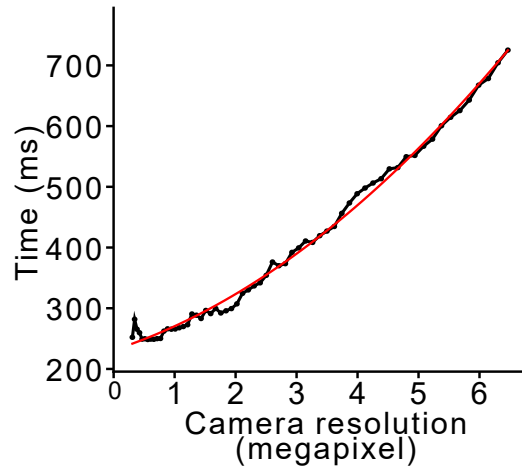


Figure 12: Latency of closed-loop control as a function of camera resolution. Red line shows a second order polynomial fit of  $y = 6.8x^2 + 32.6x + 231$ .

This means that, assuming a single-agent projection area of a single pixel, any agent moving slower than  $41\mu\text{m/s}$  could be imaged at the highest possible resolution (latency of 0.725 s) whilst maintaining accurate light projection in relation to their position. More typically, the DOME is operated at a resolution of  $1920 \times 1088$  pixels for which the latency is 0.25 s. At this resolution, agents moving slower than  $120 \mu\text{m/s}$  can be accurately tracked by projected light. For faster moving agents, lower projector resolutions can be employed, larger light projection areas used, or both. More advanced algorithms can also be used to predict the location of an agent in a subsequent frame based on its current trajectory, however, this has not been necessary for the applications we have explored.

## Implementing building blocks for collective behaviours

The ability of the DOME to interact with many microscale agents in parallel and in a closed-loop manner makes it a useful tool for the engineering of microswarms. To demonstrate this, as well as the functionality of the system more broadly, we implemented three essential building blocks for collective behaviours using the algae *Volvox* as our microagent. *Volvox* was chosen due to its innate capability to move and sense light (Drescher et al., 2010a), and because the spherical shape and size of its colonies (350-500  $\mu\text{m}$  in diameter) are easily visualised under a microscope (Figure 7).

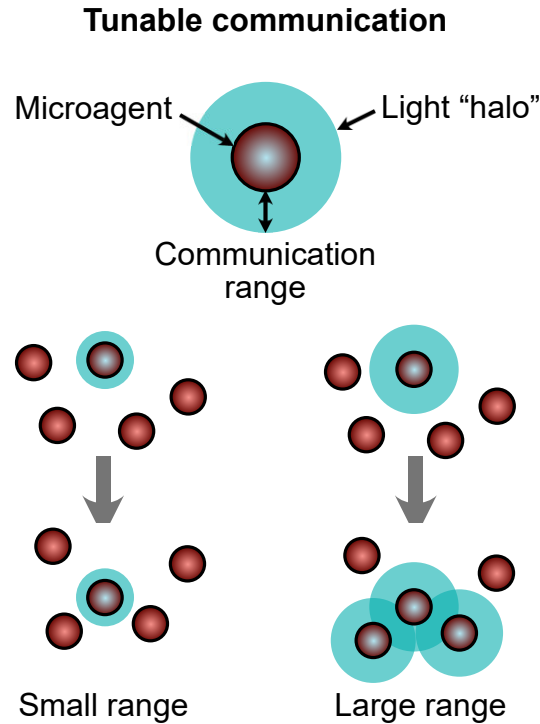


Figure 13: Schematic of light-based communication between microagents with a tuneable communication range. A larger range increases the probability of a propagation event

First, we focused on the ability to enact signalling/communication between agents and shape the spread of information through a population. Here, the signalling is an augmented process of virtual interactions, encoded as projected light halos around each *Volvox* with a tuneable range and colour (Figure 13).

Rich media available at <https://youtu.be/ytidYi-EI5M>

A light signal was transmitted to a nearby *Volvox* if they fell within the halo's extent. This 'augmented' light-based signalling mechanism allowed for a few 'seed' *Volvox* colonies that start with the signal active, to propagate the signal throughout the population as they move and interact (Figures 14 and ??) (Denniss et al., 2019). The efficiency of signal propagation is governed by the communication range, with larger ranges leading to more rapid spread.

In addition, we showed that multiple signals can propagate in parallel (Figures 15 - ??) by using different colours for each signal.

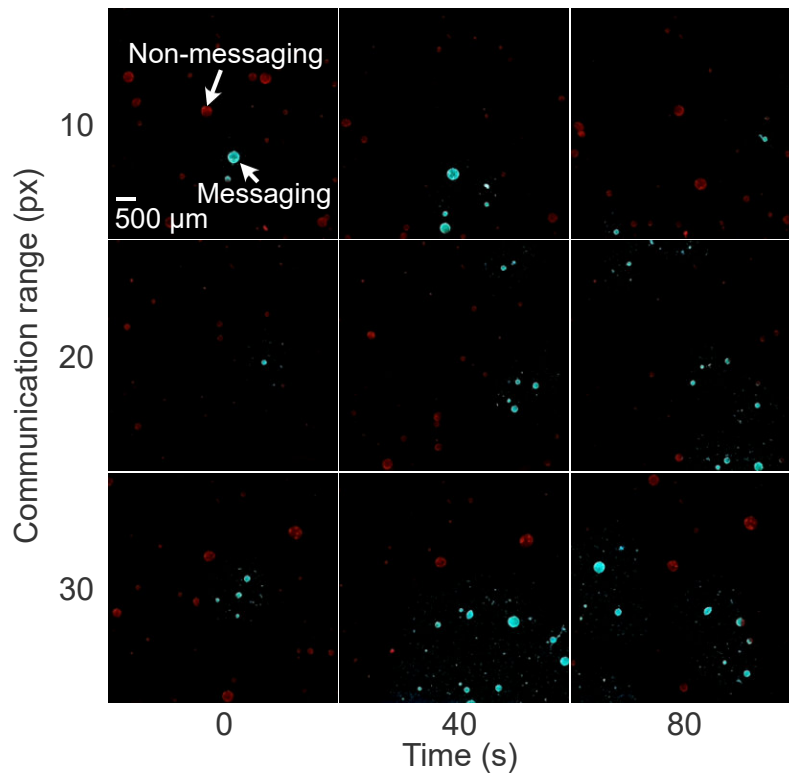


Figure 14: Image time series of light-based communication between motile *Volvox* colonies with varying communication ranges. Non-messaging *Volvox* appear in red due to illumination by a uniform red background light, while messaging *Volvox* are illuminated in cyan.

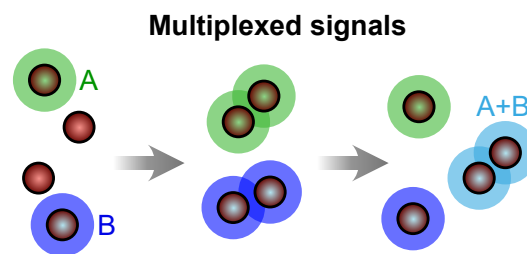


Figure 15: Schematic of multiplexed communication in which two signals (A: green, and B: blue) propagate between microagents when they are physically close to each other. When the signals interact, they create a third mixed state (A+B: cyan).

Rich media available at <https://youtu.be/FcMj0lnt6Vs>

While the *Volvox* themselves are unaware of the mechanism by which these light signals are transmitted, their motion and interactions play a direct role in the spread of signals and could offer an essential building block in collective behaviours such as consensus formation, quorum sensing, information or disease propagation, or the modelling of extracellular signalling.

Collective behaviours often rely on the ability for agents to modify their local environment through a process called stigmergy, creating a spatially distributed memory that the agents use to coordinate their actions.

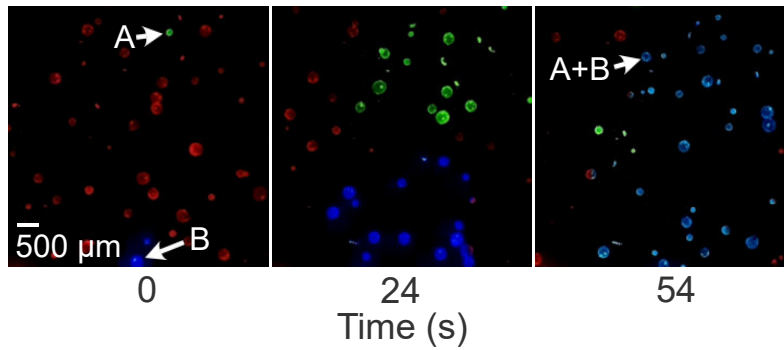


Figure 16: Image time series of multiplexed communication between *Volvox* colonies. Blue and green ‘seed’ colonies are initialised and the two signals propagate through the population until a majority of *Volvox* are in a mixed state

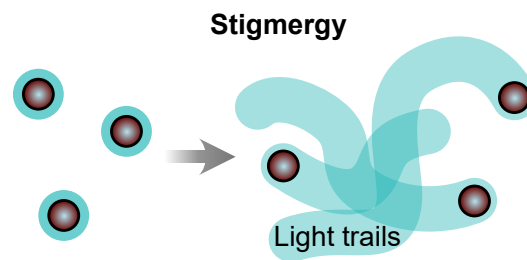


Figure 17: Schematic of light-based stigmergy in which microagents deposit light trails as they move.

As a second building block, we implemented light-based stigmergy using the DOME. This was achieved by tracking each *Volvox* colony and projecting light trails over the previous paths they had taken (Figure 17).

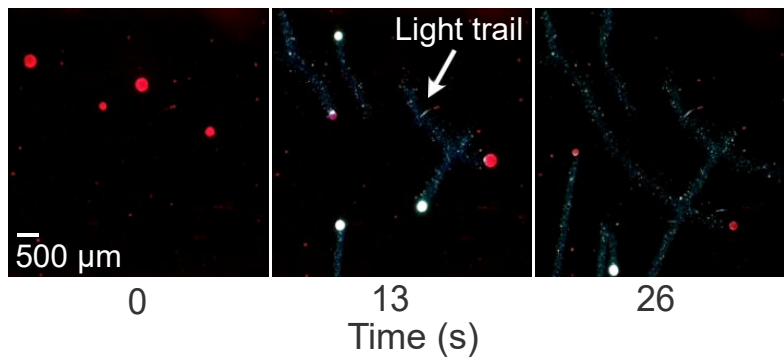


Figure 18: Image time series of light-based stigmergy with *Volvox* colonies depositing cyan light trails.

Rich media available at <https://youtu.be/AvJmGvLeUPw>

This resulted in a patchwork of light-trails emerging over time (Figures 18 and ??), reminiscent to the way ants and robot swarms lay trails to optimise foraging or area coverage (Hunt et al., 2019).

While analysing these experiments we observed that many of the moving *Volvox* slowed down when entering an illuminated path for a short period of time, before resuming their motion. It is known that *Volvox* are sensitive to light and that they reorient themselves in relation to a light signal with the goal of improving

photosynthesis (Drescher et al., 2010b). Therefore, as a final demonstration of a building block of collective behaviours, we attempted to use this innate response as a means to selectively inhibit the movement of a subset of the population.

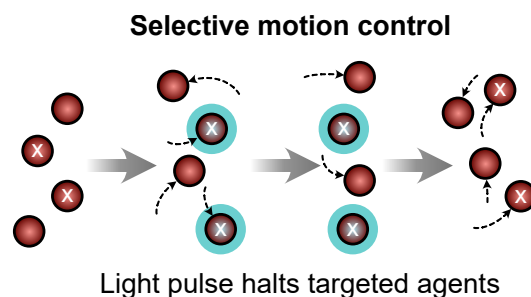


Figure 19: Schematic of selective motion control using the DOME where targeted agents (marked with white crosses) are pulsed with cyan light causing their motion to temporarily halt.

We randomly selected half of the population to be targeted and then periodically after 10 frames ( $\sim 2.5$  s) illuminated these specific colonies for 2 frames ( $\sim 0.5$  s) using cyan light that *Volvox* are known to be responsive to (Figure 19). The velocities for each colony were tracked throughout the experiment. Notably, analysis of *Volvox* motion over time showed that only targeted cells saw clear changes in velocity (slowing down) when illuminated in a punctuated fashion (Figures ?? and 20).

Rich media available at <https://youtu.be/-s8M2UwTxqY>

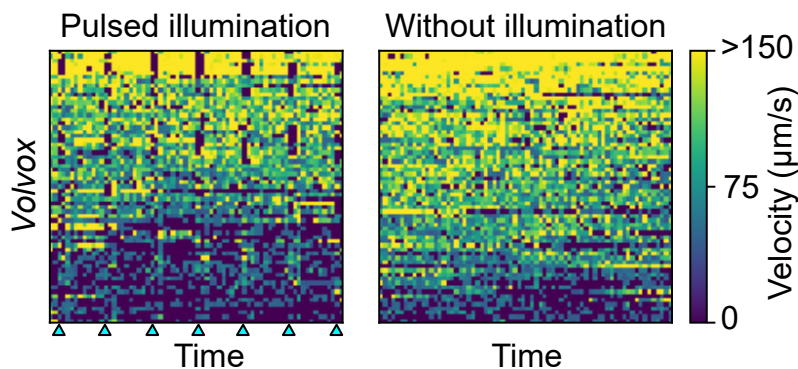


Figure 20: Heat map of experimentally measured *Volvox* colonies over a 17.5 second time course split by (left) colonies exposed to 0.5 second pulses of cyan light (start of time points denoted by triangles), and (right) those without illumination.

However, wide variability in the effect of the light pulses was also observed, with more motile *Volvox* tending to be more strongly inhibited by the light. This heterogeneity is unavoidable in biological systems, further strengthening the need for tailored control of individual agents made possible using the DOME.

## Cost and accessibility

One of the primary aims of the DOME is to provide an accessible platform for optical interaction with microscale agents. While comparative systems have been proposed previously, none provide a fully integrated

<i>Optical</i>	Cost (£)
Projector (DLP Lightcrafter Display 2000 EV, Texas Instruments)	109
Condenser lens (50mm Diameter PCX , Edmund Optics)	37
Tube lens (9X Eyepiece Cell Assembly, Edmund Optics)	61
10X objective (Semi-Plan Standard Objective, Edmund Optics)	122
Glass diffuser (DG10-1500, Thor Labs)	15
Neutral density filter (NE10B-A, Thor Labs)	47
Longpass filter (FEL0500, Thor Labs)	60
<i>Electrical</i>	
Raspberry Pi (Raspberry Pi 4 Model 4GB, The Pi Hut)	54
Raspberry Pi (Raspberry Pi Zero W, The Pi Hut)	9
Camera (Raspberry Pi Camera V2, The Pi Hut)	24
2 × SD card (SanDisk Ultra 16GB microSDHC, Amazon)	14
Interface PCB (Custom, PCBWay)	3
Power supply (UK Raspberry Pi 4 Power Supply The Pi Hut)	8
Power supply (Raspberry Pi 3 Universal Power Supply)	8
Power supply (RS Pro Plug In Power Supply 5V)	10
<i>Mechanical</i>	
PLA filament (Black Premium PLA 1.75mm, FilaPrint)	28
Linear rail set (Glvanc 3D Printer Guide Rail Sets, Amazon)	21
x-y stage (Zetiling Microscope Moveable Stage, Amazon)	15
Linear Motion Ball Bearing (LM8LUU, Amazon)	7
Lighting and fastening sundries	45
<b>Total cost</b>	<b>699</b>

Table 1: Breakdown of DOME component costs with all prices given to the nearest pound (£) and inclusive of 20% VAT.

device and most provide little to no documentation to enhance reproducibility. The DOME is truly open source, with the STL files required to fabricate the device available [online](#) along with protocols detailing the computational set up. In addition, a video tutorial showing the step by step construction process is available (Figure ??).

Rich media available at <https://youtu.be/MaPmAVyvZ1s>

The DOME is operated using control scripts written in Python for a Raspberry Pi interface, making it a highly accessible platform even for users with little or no programming experience. The cost of a DOME varies depending on the configuration, but a system capable of both 9X and 90X magnification and bright-field and fluorescence imaging comes to £699 (Table 1), making the system affordable for most labs.

## Device comparison

As a low-cost, open source and fully integrated device, the DOME demonstrates functionality of the same level or higher than comparable optical set ups of a greater cost. In Table 2, key characteristics of these systems, such as minimal pixel size and illumination wavelengths, are compared to those of the DOME. In addition, the openness of the systems, availability of documentation and cost are considered.

Of these, only the DOME is fully open and available for under £1000. The other low cost system ([Lam et al., 2017](#)) requires an external optical breadboard which is not included in the cost calculation, and the details of which are not provided in literature. This could make reproduction challenging for users without access to such equipment, and who may have limited experience with such optical systems. The only other

Ref.	Minimal pixel size ( $\mu\text{m}$ )	Illumination wave-lengths (nm)	Imaging modes	Documentation available	Open	Under £1000
( <a href="#">Rahman et al., 2017</a> )	20	1064	Unknown	Partially	No	No
( <a href="#">Palagi et al., 2016</a> )	Unknown	532	Unknown	Partially	No	No
( <a href="#">Choi et al., 2006</a> )	33	Unknown	BF	No	No	No
( <a href="#">Rullan et al., 2018</a> )	Unknown	617, 520, 465	BF, FL	Yes	No	No
( <a href="#">Frangipane et al., 2018</a> )	2	617, 520, 465	BF	Yes	No	No
( <a href="#">Chait et al., 2017</a> )	0.24	530, 660	FL	Partially	Partially	No
( <a href="#">Steager et al., 2015</a> )	1	<500	BF	No	No	No
( <a href="#">Lam et al., 2017</a> )	20	Full spectrum	BF	Partially	No	Yes*
( <a href="#">Stirman et al., 2012</a> )	5,14	430–475, 543–593, 585–670	BF	Yes	Yes	No
( <a href="#">Leifer et al., 2011</a> )	10, 30	532, 473	BF	Yes	No	No
DOME	30	460, 510, 640	BF, FL	Yes	Yes	Yes

Table 2: Summary of the key specifications of various closed-loop optical control devices comparable to the DOME. The abbreviations BF and FL here stand for bright-field and fluorescence. For one entry, marked with an asterisk (\*), the calculated cost is exclusive of the optical breadboard used to mount and align components.

fully open system ([Stirman et al., 2012](#)) is based on a fluorescence microscope, making the total system cost approximately a factor of 10 higher than that of the DOME.

## Conclusion

In summary, the DOME offers a versatile and low-cost platform for the engineering of microscopic collectives using light. The DOME's open-source modular design makes it easy to adapt for new needs, for example, changing the light source of the projector to enable different forms of fluorescent imaging, different magnification, or adding temperature/gas control to maintain the viability of different types of cell (e.g. mammalian cells), and future extensions could even introduce magnetic, sound, or chemical inputs as additional control modalities. The basic building blocks of local communication, stigmergy, and controllable motion demonstrated here using the DOME platform could be used as the basis for more complex collective behaviours. Entirely new swarm behaviours could even be engineered by combining the closed loop nature of the DOME with automatic discovery processes based on machine learning algorithms (Jones et al., 2019; Cichos et al., 2020; Solé et al., 2018). Beyond microswarm engineering, the DOME also offers a means to both understand and influence the collective behaviour of natural cellular populations, opening up new avenues for the study of complex systems spanning cancer to the microbiome.

## References

- Yunus Alapan, Oncay Yasa, Berk Yigit, I. Ceren Yasa, Pelin Erkok, and Metin Sitti. Microrobotics and Microorganisms: Biohybrid Autonomous Cellular Robots. *Annual Review of Control Robotics, and Autonomous Systems*, 2(1):205–230, may 2019. doi: 10.1146/annurev-control-053018-023803. URL <https://doi.org/10.1146/annurev-control-053018-023803>.
- Manuele Brambilla, Eliseo Ferrante, Mauro Birattari, and Marco Dorigo. Swarm robotics: a review from the swarm engineering perspective. *Swarm Intelligence*, 7(1):1–41, jan 2013. doi: 10.1007/s11721-012-0075-2. URL <https://doi.org/10.1007/s11721-012-0075-2>.
- R Chait, J Ruess, T Bergmiller, G Tkačik, and CC Guet. Shaping bacterial population behavior through computer-interfaced control of individual cells. *Nat Commun*, 8:1535, Nov 2017.
- Y Chen, Z Wang, Y He, YJ Yoon, J Jung, G Zhang, and Z Lin. Light-enabled reversible self-assembly and tunable optical properties of stable hairy nanoparticles. *Proc Natl Acad Sci U S A*, 115:E1391–E1400, Feb 2018.
- Wonjae Choi, Se-Hwan Kim, Jin Jang, and Je-Kyun Park. Lab-on-a-display: a new microparticle manipulation platform using a liquid crystal display (LCD). *Microfluidics and Nanofluidics*, 3(2):217–225, oct 2006. doi: 10.1007/s10404-006-0124-5. URL <https://doi.org/10.1007/s10404-006-0124-5>.
- Frank Cichos, Kristian Gustavsson, Bernhard Mehlig, and Giovanni Volpe. Machine learning for active matter. *Nature Machine Intelligence*, 2(2):94–103, 2020.
- Baohu Dai, Jizhuang Wang, Ze Xiong, Xiaojun Zhan, Wei Dai, Chien-Cheng Li, Shien-Ping Feng, and Jinyao Tang. Programmable artificial phototactic microswimmer. *Nature Nanotechnology*, 11(12):1087–1092, oct 2016. doi: 10.1038/nnano.2016.187. URL <https://doi.org/10.1038/nnano.2016.187>.
- Ana Maria Rubio Denniss, Thomas E. Gorochoowski, and Sabine Hauert. Augmented reality for the engineering of collective behaviours in microsystems. In *2019 International Conference on Manipulation Automation and Robotics at Small Scales (MARSS)*. IEEE, jul 2019. doi: 10.1109/marss.2019.8860907. URL <https://doi.org/10.1109/marss.2019.8860907>.
- Benedict Diederich, René Lachmann, Swen Carlstedt, Barbora Marsikova, Haoran Wang, Xavier Uwurukundo, Alexander S. Mosig, and Rainer Heintzmann. A versatile and customizable low-cost 3D-printed open standard for microscopic imaging. *Nature Communications*, 11(1), nov 2020. doi: 10.1038/s41467-020-19447-9. URL <https://doi.org/10.1038/s41467-020-19447-9>.

- K. Drescher, R. E. Goldstein, and I. Tuval. Fidelity of adaptive phototaxis. *Proceedings of the National Academy of Sciences*, 107(25):11171–11176, jun 2010a. doi: 10.1073/pnas.1000901107. URL <https://doi.org/10.1073/pnas.1000901107>.
- K Drescher, RE Goldstein, and I Tuval. Fidelity of adaptive phototaxis. *Proc Natl Acad Sci U S A*, 107: 11171–6, Jun 2010b.
- Pelin Erkoç, Immihan C. Yasa, Hakan Ceylan, Oncay Yasa, Yunus Alapan, and Metin Sitti. Mobile Microrobots for Active Therapeutic Delivery. *Advanced Therapeutics*, 2(1):1800064, oct 2018. doi: 10.1002/adtp.201800064. URL <https://doi.org/10.1002/adtp.201800064>.
- G Frangipane, D Dell’Arciprete, S Petracchini, C Maggi, F Saglimbeni, S Bianchi, G Vizsnyiczai, ML Bernardini, and Leonardo R Di. Dynamic density shaping of photokinetic E. coli. *Elife*, 7, Aug 2018.
- TE Gorochoowski, S Hauert, JU Kreft, L Marucci, NR Stillman, TD Tang, L Bandiera, V Bartoli, DOR Dixon, AJH Fedorec, H Fellermann, AG Fletcher, T Foster, L Giuggioli, A Matyjaszkiewicz, S McCormick, Olivas S Montes, J Naylor, Denniss A Rubio, and D Ward. Toward Engineering Biosystems With Emergent Collective Functions. *Front Bioeng Biotechnol*, 8:705, 2020.
- Sabine Hauert and Sangeeta N. Bhatia. Mechanisms of cooperation in cancer nanomedicine: towards systems nanotechnology. *Trends in Biotechnology*, 32(9):448–455, sep 2014. doi: 10.1016/j.tibtech.2014.06.010. URL <https://doi.org/10.1016/j.tibtech.2014.06.010>.
- ER Hunt, S Jones, and S Hauert. Testing the limits of pheromone stigmergy in high-density robot swarms. *R Soc Open Sci*, 6:190225, Nov 2019.
- Gáspár Jékely, Julien Colombelli, Harald Hausen, Keren Guy, Ernst Stelzer, François Nédélec, and Detlev Arendt. Mechanism of phototaxis in marine zooplankton. *Nature*, 456(7220):395–399, nov 2008. doi: 10.1038/nature07590. URL <https://doi.org/10.1038/nature07590>.
- Simon Jones, Alan F. Winfield, Sabine Hauert, and Matthew Studley. Onboard Evolution of Understandable Swarm Behaviors. *Advanced Intelligent Systems*, 1(6):1970062, oct 2019. doi: 10.1002/aisy.201970062. URL <https://doi.org/10.1002/aisy.201970062>.
- Amy T. Lam, Karina G. Samuel-Gama, Jonathan Griffin, Matthew Loeun, Lukas C. Gerber, Zahid Hossain, Nate J. Cira, Seung Ah Lee, and Ingmar H. Riedel-Kruse. Device and programming abstractions for spatiotemporal control of active micro-particle swarms. *Lab on a Chip*, 17(8):1442–1451, 2017. doi: 10.1039/c7lc00131b. URL <https://doi.org/10.1039/c7lc00131b>.
- FA Lavergne, H Wendehenne, T Bäuerle, and C Bechinger. Group formation and cohesion of active particles with visual perception-dependent motility. *Science*, 364:70–74, Apr 2019.
- Andrew M Leifer, Christopher Fang-Yen, Marc Gershow, Mark J Alkema, and Aravinthan D T Samuel. Optogenetic manipulation of neural activity in freely moving *Caenorhabditis elegans*. *Nature Methods*, 8(2):147–152, jan 2011. doi: 10.1038/nmeth.1554. URL <https://doi.org/10.1038/nmeth.1554>.
- Stefano Palagi, Andrew G. Mark, Shang Yik Reigh, Kai Melde, Tian Qiu, Hao Zeng, Camilla Parmeggiani, Daniele Martella, Alberto Sanchez-Castillo, Nadia Kapernaum, Frank Giesselmann, Diederik S. Wiersma, Eric Lauga, and Peer Fischer. Structured light enables biomimetic swimming and versatile locomotion of photoresponsive soft microrobots. *Nature Materials*, 15(6):647–653, feb 2016. doi: 10.1038/nmat4569. URL <https://doi.org/10.1038/nmat4569>.
- Stefano Palagi, Dhruv P. Singh, and Peer Fischer. Light-Controlled Micromotors and Soft Microrobots. *Advanced Optical Materials*, 7(16):1900370, may 2019. doi: 10.1002/adom.201900370. URL <https://doi.org/10.1002/adom.201900370>.
- Erin B Purcell and Sean Crosson. Photoregulation in prokaryotes. *Current Opinion in Microbiology*, 11(2):

- 168–178, apr 2008. doi: 10.1016/j.mib.2008.02.014. URL <https://doi.org/10.1016%2Fj.mib.2008.02.014>.
- M. Arifur Rahman, Noboru Takahashi, Kawai F. Siliga, Nigel K. Ng, Zhidong Wang, and Aaron T. Ohta. Vision-assisted micromanipulation using closed-loop actuation of multiple microrobots. *Robotics and Biomimetics*, 4(1), oct 2017. doi: 10.1186/s40638-017-0064-4. URL <https://doi.org/10.1186%2Fs40638-017-0064-4>.
- Marc Rullan, Dirk Benzinger, Gregor W. Schmidt, Andreas Miliadis-Argeitis, and Mustafa Khammash. An Optogenetic Platform for Real-Time Single-Cell Interrogation of Stochastic Transcriptional Regulation. *Molecular Cell*, 70(4):745–756.e6, may 2018. doi: 10.1016/j.molcel.2018.04.012. URL <https://doi.org/10.1016%2Fj.molcel.2018.04.012>.
- Emily R. Ruskowitz and Cole A. DeForest. Photoresponsive biomaterials for targeted drug delivery and 4D cell culture. *Nature Reviews Materials*, 3(2), jan 2018. doi: 10.1038/natrevmats.2017.87. URL <https://doi.org/10.1038%2Fnatrevmats.2017.87>.
- F Schmidt, B Liebchen, H Löwen, and G Volpe. Light-controlled assembly of active colloidal molecules. *J Chem Phys*, 150:094905, Mar 2019.
- I Slavkov, D Carrillo-Zapata, N Carranza, X Diego, F Jansson, J Kaandorp, S Hauert, and J Sharpe. Morphogenesis in robot swarms. *Sci Robot*, 3, Dec 2018.
- Ricard Solé, Aina Ollé-Vila, Blai Vidiella, Salva Duran-Nebreda, and Nuria Conde-Pueyo. The road to synthetic multicellularity. *Current Opinion in Systems Biology*, 7:60–67, feb 2018. doi: 10.1016/j.coisb.2017.11.007. URL <https://doi.org/10.1016%2Fj.coisb.2017.11.007>.
- E. B. Steager, D. Wong, N. Chodosh, and V. Kumar. Optically addressing microscopic bioactuators for real-time control. In *2015 IEEE International Conference on Robotics and Automation (ICRA)*. IEEE, may 2015. doi: 10.1109/icra.2015.7139686. URL <https://doi.org/10.1109%2Ficra.2015.7139686>.
- Jeffrey N Stirman, Matthew M Crane, Steven J Husson, Alexander Gottschalk, and Hang Lu. A multispectral optical illumination system with precise spatiotemporal control for the manipulation of optogenetic reagents. *Nature Protocols*, 7(2):207–220, jan 2012. doi: 10.1038/nprot.2011.433. URL <https://doi.org/10.1038%2Fnprot.2011.433>.
- Georgi Stoychev, Alina Kirillova, and Leonid Ionov. Light-responsive shape-changing polymers. *Advanced Optical Materials*, 7(16):1900067, 2019.
- Y Tao, HF Chan, B Shi, M Li, and KW Leong. Light: A Magical Tool for Controlled Drug Delivery. *Adv Funct Mater*, 30, Dec 2020.